1 **Variations of the crustal thickness in Nepal Himalayas based on tomographic inversion of**

2 **regional earthquake data**

3

4 **Ivan Koulakov[1,2], Gulzhamal Maksotova[1,2], Sagarika Mukhopadhyay[3], Javed Raoof[3], J R**

5 **Kayal[4], Andrey Jakovlev[1,2] and Alexandr Vasilevsky[1,2]**

6

7

8 [1] Trofimuk Institute of Petroleum Geology and Geophysics SB RAS, Prospekt Koptyuga, 3,

9 630090, Novosibirsk, Russian Federation, email: KoulakovIY@ipgg.sbras.ru, maks_gul@mail.ru,

10 JakovlevAV@ipgg.sbras.ru

11 [2] Novosibirsk State University, Novosibirsk, Russia, Pirogova 2, 630090, Novosibirsk, Russia

12 [3] Department of Earth Sciences, IIT Roorkee, Roorkee, India, Email: sagarfes@iitr.ac.in

13 [4] School of Oceanographic Studies, Jadavpur University, Kolkata 700032, India, Email:

14 jr.kayal@gmail.com

15 Correspondence to: I. Koulakov (KoulakovIY@ipgg.sbras.ru)

16

17   Submitted to Solid Earth

18

19

20

21

22   Novosibirsk (Russia), Roorkee, Kolkata (India)

23   December, 2014

24

25

Abstract

We estimate variations of the crustal thickness beneath the Nepal Himalayas based on tomographic inversion of regional earthquake data. We have obtained a low-velocity anomaly in the upper part of the model down to depths of 40 to 80 km and proposed that the lower limit of this anomaly represents variations of the Moho depth. This statement was supported by results of synthetic modeling. The obtained variations of crustal thickness match fairly well with the free-air gravity anomalies: thinner crust patterns correspond to lower gravity values and vice versa. There is also some correlation with magnetic field: higher magnetic values correspond to the major areas of thicker crust. We propose that elevated magnetic values can be associated with more rigid segments of the incoming Indian crust which cause more compression in the thrust zone and leads to stronger crustal thickening.

1. Introduction

Collision processes are related to the convergence of continental blocks and lead to significant shortening and thickening of the crust. The collision zones with strong seismic activity often coincide with highly populated areas, leading to damage and destruction of human habitation and suffering of population. The Himalayas, which are the highest mountain chain on the Earth, has been formed due to the collision of the Indian and Asian plates. The mechanisms of mountain building in Himalayas and Tibet are extensively discussed by many authors for decades (e.g., Dewey and Bird, 1970; Seeber et al., 1981; Molnar and Tapponier, 1975; Allegre et al. 1984). As the Indian landmass moved northwards the sedimentary piles with its older crystalline foundation complexly folded, faulted and thrusted, that caused varied crustal structure all along the 2500 km long Himalayan arc from west to east. According to the most popular tectonic model of Himalayan collision (Seeber et al., 1981), the Indian plate underthrusts the Asian plate along a gentle north dipping (4-10º N) detachment plane, called the Main Himalayan Thrust (MHT) (Figure 1). Most of the Himalayan earthquakes are shallow and occur at 15 to 20

2

km depth on the MHT. Several recent seismological studies, however, suggest that the tectonic model varies from west to east. For example, earthquakes in the eastern Himalaya tend to be much deeper than in the western part (Kayal, 2001 and 2010; Mukhopadhyay and Sharma, 2010). More definitive geodynamic concepts can only be constructed based on reliable information on the deep structures in the crust and the mantle. However, due to many political and natural reasons the Himalayas is a difficult region to make a detailed study with most of geophysical methods.

The Mohorovicic (Moho) discontinuity depth is one of the key types of information which is directly linked with the major geodynamical processes. For the Himalayas, the existing Moho depth models are either too generalized or too fragmentary. For example, an existing global model CRUST2.0 (Bassin et al., 2000) provides an over smoothed solution in Himalayas with extrapolation in some parts. The gravity modeling in the Himalayas also provides fairly smooth variations of the Moho depth (e.g., Tenzer and Chen, 2014). Another gravity study by Jin et al., (1996) reported that the Moho depth varies from 38 km below Indo-Gangetic Alluvial Plains (IGAP) to about 75 km below high Himalayas. The regional tomography models though depict reliable images of the lithospheric behavior beneath Himalayas and Tibet (e.g., Li et al., 2008; Koulakov, 2011), but they cannot provide much constraints on the crustal structures. On local scale, the existing receiver function sites, deep sounding profiles and local earthquake tomography results from east to west of the Himalayas and Tibet (e.g. Kind et al., 2002; Kumar et al., 2005; Galve et al., 2002; Hauck et al., 1998; Mitra et al., 2005; Ramesh et al., 2005; Schulte-Pelkum et al., 2005; Rai et al., 2006, Mukhopadhyay and Sharma, 2010) provide reliable, but too local and sparse information which is hard to be used to build a generalized crustal model for the entire Himalayas.

In this paper we make an attempt to estimate the variations of the crustal thickness based on results of tomography inversion using the travel time data recorded by the networks of Nepal

and northern India. In most cases, seismic tomography is used to derive smooth velocity distributions and appears to be not sensitive to sharp first-order interfaces. However, in some cases it can provide useful information to estimate the variations of the main interfaces. For example, Koulakov and Sobolev (2006) provided the map of the Moho depth beneath the Middle East area based on the inversion of the regional travel time data from the ISC catalogue. This model is fairly corroborated by later studies based on receiver functions and active seismic profiles (Mechie et al., 2013). Koulakov and Sobolev (2006), however, put forward some conditions which would make possible studying the Moho depth using travel time tomography: (1) stations in the study area should be distributed densely and uniformly as much as possible; (2) sufficient amount of sources should be located inside the study region; (3) size of the area should be in the range of 150-500 km; (4) both travel times of crustal (Pg, Sg) and mantle (Pn, Sn) rays should be presented in the dataset. To some extent, all these conditions are fulfilled in the Nepal Himalayas region. Thus, we claim that the tomographic results in this study provide new information on the variations of the Moho depth beneath the Nepal Himalayas.

2. Data analysis and tomography model

We have combined the data of regional networks in northern India (run by India Meteorological Department, IMD) and Nepal (run by the Department of Mines and Geology, Nepal, DMN) along with the global ISC catalogue for the years of 2004-2014. In total, we used the information from 78 seismic stations installed in India and Nepal. The data selection was based on three criteria: (1) the residuals for the P- and S data after location of sources in the 1D model should not exceed 2 s and 3 s, respectively; (2) the number of picks per event should not be less than 8; (3) the distance from an event to the nearest recording station should not be more than 250 km. In total, 10864 P- and 5293 S arrival times from 821 events in the study region were selected for this study (on average, almost 20 picks per event). The distributions of stations

102 and selected events used for computations are shown in Figure 1. Note that only in Nepal we

103 have fairly dense distributions of both stations and earthquakes. In China to the north, there were

104 many events, but no stations were available; in India, there were some stations available, but a

105 very few events were reported.

106   The analysis of data is performed using the iterative tomographic algorithm LOTOS

107 (Koulakov, 2009). Because of the large size of the area, we have modified the code by taking

108 into account the sphericity of the Earth. All the calculations are performed in the Cartesian

109 coordinates. However, the reference model is kept radially symmetric, and Z-coordinates for the

110 events and stations are corrected according to the spherical shape of the Earth. In other aspects,

111 the workflow of the analysis was similar to that used in other studies based on this algorithm

112 (e.g., Koulakov et al., 2010). The processing starts with preliminary source locations with the use

113 of reference table containing travel times in the 1D model. In the next step, the sources are re-

114 located using 3D algorithm of ray tracing based on bending method. The velocity distributions

115 are parameterized with nodes distributed inside the study area according to the ray density. To

116 avoid any bias of the model due to predefined parameters of the grid, we performed the

117 inversions for four different grids with different basic orientations. Examples of node

118 distributions for two grids with basic orientations of 0° and 45° are shown in Figure 2. Note that

119 in map view, the node projections look regularly spaced. However, along the vertical lines, the

120 number of nodes and spacing depend on the data distribution (cases with denser node

121 distributions are depicted with darker points in Figure 2). The inversion was performed

122 simultaneously for the 3D P- and S-velocity distributions, source parameters and station

123 correction. The matrix was inverted using the LSQR method (Paige and Saunders, 1982; Nolet,

124 1987). The inversion results obtained using differently oriented grids are averaged into one

125 model which then used to update the 3D model for the next iteration. In total, for the analysis of

both synthetic and observed data, we used three iterations, each of which included the steps of source locations in the updated velocity models, matrix calculations and inversions.

To avoid any predefinition for the Moho depth, we set the reference model without any sharp interfaces and even without high gradient levels. We defined a constant Vp/Vs ratio equal to 1.75 and set the P-velocity values at different depth levels: 5 km/s at -1 km, 6 km/s at 25 km, 7.2 km/s at 40 km, 7.7 km/s at 65 km , 8 km/s at 120 km and 8.2 km/s at 210 km depth. Between these levels, the velocity was linearly interpolated. Starting velocities for P and S models are shown in Figure 3 with dotted lines.

Unlike the tomography algorithms used by Koulakov and Sobolev (2006) for studying the Moho depth in the Middle East, here we do not parameterize the Moho as a sharp first order interface with variable depth. Instead, we derive the geometry of Moho based on consideration of velocity anomalies and absolute velocities. In the starting 1D model the velocity around the Moho depths was faster than expected crustal velocities and slower than mantle velocities. As a result, the crust was revealed as low-velocity anomaly, whereas the uppermost mantle is associated with high-velocity anomaly. The variation of thickness of the crust-related low-velocity anomaly may represent the perturbations of the Moho depth. After inversion, absolute velocity forms a zone of higher gradient around the presumed location of the Moho interface, as seen in representation of average absolute velocities in Figure 3. Note that in this case we present an average for a long profile, for which the crustal thickness may vary significantly. For local points, the Moho-related high-gradient zone is seen more prominently.

To examine the adequacy of the detection of crustal thickness, we have performed a series of synthetic tests. In Figures 4A and 5 we present result of one of the tests. The synthetic model was defined as a superposition of a reference 1D velocity model and a low-velocity anomaly with the amplitude of -15% of variable thickness representing the crust. The lower limit of this anomaly is indicated in vertical sections in Figure 5 with solid lines. In map view (Figure

4A), a zone of variable thicker crust is highlighted with dotted line. Outside this zone, the Moho is set at 30 km depth. Note that starting 1D model for the synthetic reconstruction was different of the "true" reference models. This represents the realistic situation in the case of observed data analysis when the true reference model is unknown.

To compute the synthetic data, we have used the same source-receiver pairs as in the case of the real data analysis. The computed synthetic travel times were perturbed with random noise having average deviation of 0.1 s which enables approximately the same variance reduction as in the case of observed data inversion. After computing synthetic travel times using the 3D ray tracer, we "forgot" all information on the velocity distributions and source locations. Then we performed the full data processing including the steps of source locations. The restored anomalies at 35 km depth are shown in Figure 4A. In vertical sections in Figure 5, we present the restored relative anomalies and absolute velocities. It is seen that in Section 1 along Himalayas, the thickness of the derived low P-velocity anomalies correctly represents the undulations of the Moho interface in the input model, especially in the eastern part of the profile. We see that the location of the "true" Moho better corresponds to the velocity of 7.4 km/s (yellow zone) in the restored absolute velocity model.

For the Sections 2 to 5, the low-velocity anomaly is visible only beneath Nepal. Neither in the Indian nor in the Tibetan side, the crust-related anomaly is restored. This test shows that the robust reconstruction of the Moho depth using the tomographic reconstruction can be achieved only in case of coexistence of stations and events in a sufficiently large area. Just availability of only stations (like in India) or only seismicity (in Tibet) is not enough for this purpose. The resolved area can be estimated from this test that roughly coincide with the shape of the restored crust-related anomaly.

The horizontal resolution is examined with another synthetic test which is presented in Figure S1 of Supplementary materials.

As was earlier mentioned, for the inversion of the observed data, we used three iterations. During the inversion procedure, the residuals reduced from 0.807 s to 0.500 s for the P-data (37.99% of reduction) and from 1.57 s to 0.83 s for the S-data (47.14% of variance reduction). Note that the similar remnant residuals were obtained in the final synthetic model discussed above.

The results of tomographic inversions for P-velocity are presented in five vertical sections: one along and four sections across Himalayas. We present both relative deviations in respect to the starting model (Figure 6) and absolute velocities (Figure 7). In addition, one horizontal section of P-velocity anomalies at 35 km depth is presented in Figure 4B. More horizontal sections, as well as S-velocity anomalies, are presented in supplementary materials in Figure S2. We have defined the resolved area according to the results of various synthetic tests, mainly based on the capacity to retrieve crustal related anomalies in the test shown in Figure 4. Areas with lower resolution in sections 2 to 5 are shaded in the resulting plots in Figures 6 and 7.

As we see from the results of the synthetic test, thickness of the low-velocity anomaly beneath Nepal may represent the depth variations of Moho. We can also identify Moho in a zone of generally higher gradient of the absolute velocity, which is observed in plots of absolute velocities in Figure 7. Based on the results of synthetic modeling, we have identified the Moho depth approximately at the contour line of 7.4 km/s (yellow zones in Figure 7).

We have manually traced the lower limit of this low-velocity anomaly in 21 vertical sections passing across the Himalayan chain (see Figure S3 in supplementary) and created the 2D surface of this limit beneath Nepal (Figure 8A). Projections of this surface to the vertical sections below Nepal, where a satisfactory resolution is achieved, are shown in Figures 6 and 7 with solid lines. It should be noted that the unambiguous tracing of the Moho is not possible everywhere. For example in Sections 5 to 7 below the main low-velocity anomaly, there is another low-velocity pattern which appears to be weaker and separated from the upper one. This

transitional anomaly may or may not be included to the crust. In case it is included, the total thickness of the crust in the frontal zone beneath Himalayas may reach 80 km (see Figures S3 and S4 of supplementary materials) that seems to be less plausible. Thus the latter model may be accepted as more realistic model; the former one is shown in supplementary. Thick transitional zone in this area may represent underthrusting of one continental block underneath another one which results at doubling of the crustal thickness. However, as shown by synthetic tests, the resolution in this part of the area is not high; thus, we should be prudent and avoid too speculative interpretations.

In sections 4 and 5, we can compare our results with Moho depth determinations obtained in other studies. In Section 4, dotted line depicts the Moho depth derived from combined interpretation of receiver function, gravity and thermomechanical modeling by (Hetényi et al., 2006). Same as in our results, they depict flat Moho in the area where our model is resolved. To the north, their model shows gradual thickening of the crust, however this trend is observed outside the resolved area of our model. In Section 5, we can compare with the Moho depth determined from receiver functions by (Schulte-Pelkum et al., 2005). This model shows generally same dipping trend as in our result. In both profiles, Moho interface in our results appear to be deeper to 5-7 km than one determined by other authors. We should emphasize that the absolute values of Moho depth derived from tomography should be considered with prudence because of unambiguity of the conversion of continuous seismic anomalies into the interface. The relative variations of the crustal thickness, however, appear to be correct.

3. Discussion

The variations of the crustal thickness in the frontal zone of the Himalayan thrust belt, as seen in our tomographic model (Figure 8A), may be attributed to variable mechanical properties of the collided plates. The existence of weaker or more rigid segments in the underlying Indian

226 plate may cause weaker or stronger folding in the Himalayan thrust zone. However, due to

227 several reasons, it is not easy to quantify this correlation because the Indian plate is mostly

228 covered by thick sediments of the Gangetic alluvium, which hide major tectonic features.

229 To identify hidden crustal structures, the observations of potential fields might be useful.

230 In Figure 8B we show the free-air gravity anomalies for the Nepal Himalayas region extracted

231 from the global model by Andersen et al. (2010); the smoothed anomaly is obtained using a

232 Pseudo-Gaussian weight function with the characteristic radius of 10 km. In the Nepal

233 Himalayas, the gravity field demonstrates very strong variations. To the south of the Himalayas,

234 there is a strong negative anomaly, which is partly caused by isostatic compensation related to

235 the mountain growth, and it might also reflect thick sediments of the Gangetic alluvium brought

236 from the Himalayas due to very fast erosion. The maximum value of the free-air gravity field is

237 observed in the higher Himalayas along the Nepal - China border. It is clear that these strong

238 variations across the Himalayan thrust zone are mostly due to abrupt Moho dipping from

239 relatively thinner crust in the Indian Plate to almost doubled crust beneath the Himalayas and

240 Tibet. Along the Himalayas we also observe strong variations of the gravity anomalies which

241 might be associated with laterally inhomogeneous thickness of the crust. The lateral variations in

242 gravity anomalies in Nepal correlate rather well with our estimates of the crustal thickness. For

243 example, areas of thinner crust indicated with "1", "3", "6" and "8" correspond to lower-gravity

244 anomaly patterns. On the contrary, thicker crust segments numbered with "2", "4", "5", "7" and

245 "9" are associated with higher ~~values of~~ gravity anomalies.

246 Here we also examine the magnetic anomalies extracted from the global compilation by

247 Maus et al. (2009). Besides the map for the Nepal Himalayas and adjacent areas in Figure 8c, we

248 present the map of magnetic anomalies for a much larger area in Figure S5 of supplementary. In

249 the Nepal Himalayas, the correlation of crustal thickness with the magnetic anomalies is not as

250 clear as found with the gravity map (partly due to non-availability of high-resolution magnetic

data in Nepal). However, it is worth noting that the largest pattern of thinner crust "6"
corresponds to the negative magnetic anomaly. On the contrary, the positive anomaly "4" in the
frontal thrust zone is located close to the positive magnetic anomaly to the south.

Based on the observed correlation of the seismic model with gravity and magnetic
anomalies, we propose a mechanism which may explain the variability of crustal thickness along
the Nepal Himalayas. As observed in regional magnetic map of India (Figure S5 of
supplementary), the crust of the Indian plate appears to be much heterogeneous. One of the
reasons for strong magnetic anomalies may be the presence of large provinces affected by relict
igneous processes. Although these occurred in the geological past, the large magmatic intrusions
might considerably strengthen the crust. The negative magnetic anomalies, on the other hand,
may be explained by thicker sediments. In case of collision, these two types of the crust behave
differently and cause different mechanical effect. The crust affected by igneous processes is
stronger and thus the compression of the overlying crust in the collision zone would be more
prominent. This would explain the thicker crust in anomaly "4" close to the contact area, which
can be explained by stronger pushing effect of more rigid partition of the Indian plate. The
presence of southward curve of the mountain limit line in front of the thicker crustal pattern "4"
may represent a broader shortening zone produced by the more rigid incoming block. The
segment of the anomalously thinner crust "6" may be explained by smaller compression rate of
the crust because of weaker incoming crust and lubricating effect of thicker sediments having
lower magnetic effect. In this case, the mountain front line is curved northward indicating less
intensive shortening.

4. Conclusions

In most tomographic studies, the main target is the smooth distribution of seismic
properties which is not sensitive to the geometry of first-order interfaces. In this study we made

an attempt to reconstruct variations of the Moho interface beneath the Nepal Himalayas where more or less uniform distribution of stations and sources take place and travel times of both crustal (Pg, Sg) and mantle rays (Pn, Sn) are available. Based on synthetic modeling, we found that for the most of the Nepal Himalayas area, the crustal thickness variations can be robustly retrieved. For the surrounding areas, like northern India and Tibet, crustal structures cannot be resolved with the available data.

The obtained crustal thickness varies from 40 to 75 km along the Nepal Himalayas. There is a fair correlation of the derived crustal structures with the observed gravity and magnetic anomalies. The areas of thicker crust are associated with higher values of the free-air gravity field and vice versa. This correlation is a good argument to prove the reliability of our findings. The magnetic anomalies may provide important information on the mechanical properties of the crust. We see that different segments of the Indian crust behave differently leading to various collision rates. We expect that thicker crust in the frontal thrust zone can be associated with the more rigid incoming crust. Weaker crust segments may penetrate underneath overlying plate with less resistance, and thus the weaker compression rate leads to thinner crust in the frontal thrust zone. The presence of thick sediments may have a lubricating effect and thus may also reduce the shortening of the crust.

This study gives us a fair understanding of the Moho configuration beneath the central Himalayas. However, western and eastern parts of the Himalayas are not yet well studied. Such comprehensive study based on joint consideration of seismic, gravity and magnetic data for the entire Himalayas will make possible better understanding the mechanisms of the India – Asia collision.

Authors contribution:

300   J. R. and S. M. provided seismic data and performed its preliminary analysis and

301 preparation. G. M. with help of A. J. performed all tomographic calculations. A. V. provided

302 necessary data and information on magnetic and gravity fields used in the paper. J. R. K., S. M.

303 and I. K. provided geodynamical interpretation of presented results. A. J. prepared presented

304 graphic materials. I. K. prepared manuscript with contributions of all co-authors.

305

310

311 **References:**

312 Allegre, C. O., Courtillot, V., Tapponnier, P., Hirn, A., Mattauer, M., Coulon, C., and Xu, R.:

313   Structure and evolution of the Himalaya – Tibet Organic Belt, Nature, 30, 17-22, 1984.

314 Andersen, O. B., Knudsen, P., and Berry, P.: The DNSC08GRA global marine gravity field from

315   double retracked satellite altimetry, Journal of Geodesy, Volume 84, Number 3, doi:

316   10.1007/s00190-009-0355-9, 2010.

317 Baruah, S., Saikia, S., Baruah, S., Bora, P. K., Tatevossian, R., and Kayal, J. R.: The September

318   2011 Sikkim Himalaya earthquake Mw 6.9: is it a plane of detachment earthquake?

319   Geomatics, Natural Hazards and Risk, 1-17, doi: 10.1080/19475705.2014.895963, 2014

320 Bassin, C., Laske, G., and Masters, G.: The current limits of resolution for surface wave

321   tomography in North America, EOS, Trans. AGU, 81, F897, 2000.

322 Dewey, J. F., and Bird, J. M.: Mountain belts and the new global tectonics, Journal of

323   Geophysical Research, 75(14), 2625-2647, 1970.

Galvé, A., Sapin, M., Hirn, A., Diaz, J., Lépine, J. C., Laigle, M., Gallart, J., and Jiang, M.: Complex images of Moho and variation of Vp/Vs across the Himalaya and South Tibet, from a joint receiver-function and wide-angle-reflection approach, Geophysical Research Letters, 29, no. 24, 35-1, 2002.

Gansser, A.: The Geology of the Himalayas, Wiley Interscience, London, 289 p., 1964.

Hauck, M. L., Nelson, K. D., Brown, L. D., Zhao, W., and Ross, A. R.: Crustal structure of the Himalayan orogen at 90º east longitude from Project INDEPTH deep reflection profiles, Tectonics, 17(4), 481-500, 1998.

Hetényi, G., Cattin, R., Vergne, J., and Nábělek, J. L.: The effective elastic thickness of the India Plate from receiver function imaging, gravity anomalies and thermomechanical modelling. Geophysical Journal International, 167(3), 1106-1118, 2006

Jin, Y., Mcnutt, M. K., and Zhu, Y.-S.: Mapping the descent of Indian and Eurasian plates beneath the Tibetan plateau from gravity anomalies, J. Geophys. Res., 101 B5 : 11,275 – 11,290, 1996.

Kayal, J. R.: Microearthquake activity in some parts of the Himalaya and the tectonic model, Tectonophysics, 339(3), 331-351, 2001.

Kind, R., Yuan, X., Saul, J., Nelson, D., Sobolev, S.V., Mechie, J., Zhao, W., Kosarev, G., Ni, J., Achauer, U., and Jiang, M.: Seismic images of crust and upper mantle beneath Tibet: Evidence for Eurasian plate subduction, Science, 298, 1219-1221, 2002.

Koulakov, I.: LOTOS code for local earthquake tomographic inversion. Benchmarks for testing tomographic algorithms, Bulletin of the Seismological Society of America, Vol. 99, No. 1, 194-214, doi: 10.1785/0120080013, 2009.

Koulakov, I.: High-frequency P and S velocity anomalies in the upper mantle beneath Asia from inversion of worldwide traveltime data, J. Geophys. Res., 116, B04301, doi:10.1029/2010JB007938, 2011.

349 Koulakov, I., and Sobolev, S. V.: Moho depth and three-dimensional P and S structure of the

350   crust and uppermost mantle in the Eastern Mediterranean and Middle East derived from

351   tomograpic inversion of local ISC data, Geophysical Journal International, 164, 1, 218-235,

352   2006.

353 Koulakov, I., Zaharia, B., Enescu, B., Radulian, M., Popa, M., Parolai, S., and Zschau, J.:

354   Delamination or slab detachment beneath Vrancea? New arguments from local earthquake

355   tomography, G-cubed, 10, Q03002, doi:10.1029/2009GC002811, 2010.

356 Kumar, P., Yuan, X., Kind, R., and Kosarev, G.: The lithosphere-asthenosphere boundary in the

357   Tien Shan-Karakoram region from S receiver functions: Evidence for continental

358   subduction, Geoph. Res. Lett., 32, L07305, doi: 10.1029/2004GL022291, 2005.

359 Li., C., van der Hilst, R. D, Meltzer, A. S., and Engdahl, E. R.: Subduction of the Indian

360   lithosphere beneath the Tibetan Plateau and Burma, Earth Planet Sci Lett., 274(1), 157-

361   168. doi:10.1016/j.epsl.2008.07.016, 2008.

362 Maus, S., Barckhausen, U., Berkenbosch, H., Bournas, N., Brozena, J., Childers, V., Dostaler, F.,

363   Fairhead, J. D., Finn, C., von Frese, R. R. B., Gaina, C., Golynsky, S., Kucks, R., Lühr, H.,

364   Milligan, P., Mogren, S., Müller, R. D., Olesen, O., Pilkington, M., Saltus, R.,

365   Schreckenberger, B., Thébault, E. and Caratori Tontini, F.: EMAG2: A 2–arc min

366   resolution Earth Magnetic Anomaly Grid compiled from satellite, airborne, and marine

367   magnetic measurements, Geochemistry, Geophysics, Geosystems, 10(8), 2009.

368 Mechie, J., Ben-Avraham, Z., Weber, M., Götze, H.-J., Koulakov, I., Mohsen, A., and Stiller,

369   M.: The distribution of Moho depths beneath the Arabian plate and margins,

370   Tectonophysics, 609, 234-249, doi:10.1016/j.tecto.2012.11.015, 2013.

371 Mitra, S., Priestley, K., Bhattacharyya, A. K., and Gaur, V. K.: Crustal structure and earthquake

372   focal depths beneath northeastern India and southern Tibet, Geophysical Journal

373   International, 160(1), 227-248, 2005.

374   Molnar, P., and Tapponnier, P.: Cenozoic tectonics of Asia: Effects of a continental collision,

375   Science, 189(4201), 419-426, 1975.

376   Mukhopadhyay, S., and Sharma, J.: Crustal scale detachment in the Himalayas: a reappraisal,

377   Geoph. J. Int., 183, 850–860, doi: 10.1111/j.1365-246X.2010.04755.x, 2010

378   Nakata, T.: Active fault of the Himalayas of India and Nepal, In: Tectonics of Western

379   Himalayas, Eds. Malinconico Jr., L.L. and Lillie R., Geol. Soc. Am. Sp. Pap., 232, 243-

380   264, 1989.

381   Ni, J. F.: Active tectonics of the Himalaya, Proc. Indian Acad. Sci. (Earth Planet Sci), 98, 71-89,

382   1989.

383   Nolet, G.: Seismic wave propagation and seismic tomography, in: Nolet, G. (ed.), Seismic

384   Tomography, Reidel, Dordrecht, 1-23, 1987.

385   Paige, C. C., and Saunders, M. A.: LSQR: An algorithm for sparse linear equations and sparse

386   least squares, ACM Trans. Math. Soft, 8, 43-71, 1982.

387   Ramesh, D. S., Kumar, M. R., Devi, E.U., Raju, P.S., and Yuan, X.: Moho geometry and upper

388   mantle images of northeast India, Geophys. Res. Lett., 32, 14301-14304, doi:

389   10.1029/2005GL022789, 2005.

390   Rai, S. S., Priestley, K., Gaur, V. K., Mitra, S., Singh, M. P., and Searle, M.: Configuration of

391   the Indian Moho beneath the NW Himalaya and Ladakh, Geophysical Research Letters, 33:

392   doi: 10.1029/2006GL026076, issn: 0094-8276, 2006.

393   Schelling, D.: The tectonostratigraphy and structure of the eastern Nepal Himalaya, Tectonics,

394   11, 925-943, 1992.

395   Schulte-Pelkum, V., Sheehan, A., Wu, F., and Billham, R.: Imaging the Indian subcontinent

396   beneath the Himalaya, Nature, 435, 1222-1225, 2005.

397 Seeber, L., Armbruster, J. G., and Quittmeyer, R.: Seismicity and continental subduction in the

398   Himalayan Arc, In: Zagros, Hindu Kush, Himalaya, Geodynamic Evolution, Geodyn. Ser.

399   Vol. 3, Eds. Gupta, H.K. and Delany, F.M., pp. 215-242, 1981.

400 Tenzer, R., and Chen, W.: Regional gravity inversion of crustal thickness beneath the Tibetan

401   plateau, Earth Science Informatics, 1-12, 2014.

402 Valdiya, K.S.: Himalayan transverse faults and their parallelism with subsurface structures of

403   north Indian plains, Tectonophysics, 32, 352-386, 1976.

404

405 **Figure captions:**

406 Figure 1. Map of the study area and data distrubutions. Background is topography. Yellow dots

407   are the earthquakes, and red triangles are the stations used in this study. Locations of three

408   profiles used for visualization of the results are shown. Blue lines indicate the Main

409   Centran Thrust (MCT) and the Main Boundary Thrust (MBT). IGAP is the Indo-Gangetic

410   Alluvial Plains. Inset shows the location of the region.

411 Figure 2. Distribution of P-rays and two parameterization grids corresponding to basic

412   orientations of 0 and 45 degrees.   Intensity of the points represents the number of nodes in

413   Z-direction corresponding to the current XY coordinates.

414 Figure 3.   P- and S-velocity versus depth. Dotted lines depict starting 1D velocity models, solid

415   line represents average velocities along section 1for the main result shown in Figures 6-7.

416 Figure 4. Velocity anomalies at 35 km depth after inversion of synthetic (A) and observed data

417   (B). For the case of synthetic modeling, the limits of "thick crust" are marked with dotted

418   line. Triangles denote stations. Locations of profiles presented in Figures 3 to 5 are shown.

419 Figure 5. Synthetic test with reconstruction of the "variable Moho" model in relative anomalies

420   (upper part) and absolute P-velocities (lower part). Locations of the profiles are shown in

421   Figure 2. The configuration of the synthetic "Moho" is indicated with dotted line. Vertical

422   lines with numbers mark locations where sections cross each other.

423   Figure 6. Vertical sections of the resulting P-velocity anomalies. Locations of sections are

424   indicated in Figure 4. Above each section, exaggerated topography is shown. Vertical lines

425   indicate locations where sections cross each other. Areas with poorer resolution in sections

426   2 to 5 are shaded. Moho interface (black line) is traced on the bottom of the low-velocity

427   anomaly. Dashed line in Sections 1 and 2 indicates an alternative interpretation which is

428   less plausible. Dotted lines in Sections 4 and 5 indicate Moho depth determinations from

429   (*Hetényi et al.,* 2006) and (*Schulte-Pelkum et al.,* 2005), respectively. More sections are

430   shown in Supplementary.

431   Figure 7. Same as Figure 6, but for absolute P-velocity.

432   Figure 8. Map of estimated Moho depth beneath the Nepal Himalayas (A) together with free-air

433   gravity anomalies (*Andersen et al.,* 2010) (B) and magnetic anomalies (*Maus et al.,* 2009)

434   (C). Red numbers indicate the locations discussed in the text. In Plot A, the locations of

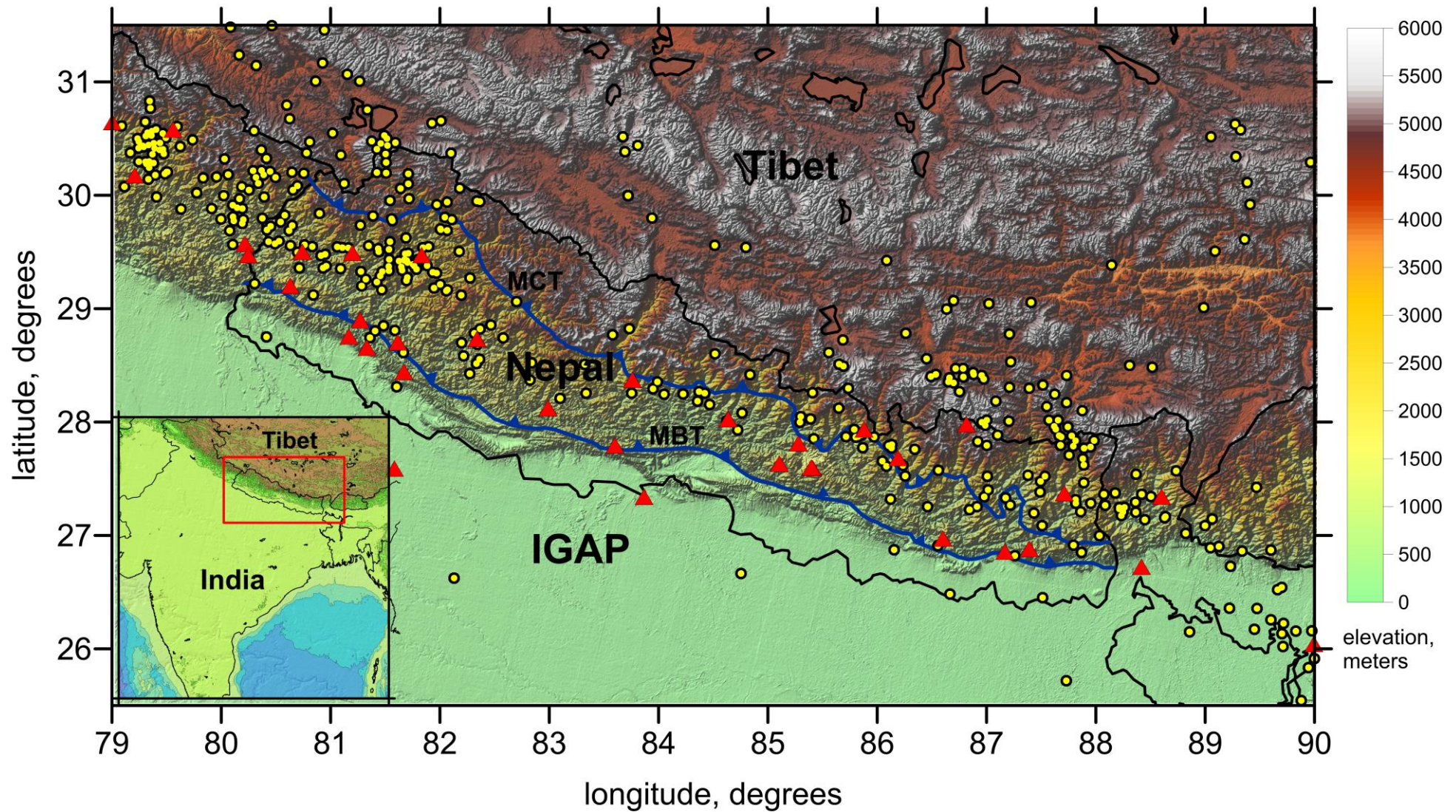435   profiles used for presenting the main results are shown.

Figure 1. Map of the study area and data distrubutions. Background is topography. Yellow dots are the earthquakes, and red triangles are the stations used in this study. Locations of three profiles used for visualization of the results are shown. Blue lines indicate the Main Centran Thrust (MCT) and the Main Boundary Thrust (MBT). IGAP is the Indo-Gangetic Alluvial Plains. Inset shows the location of the region.
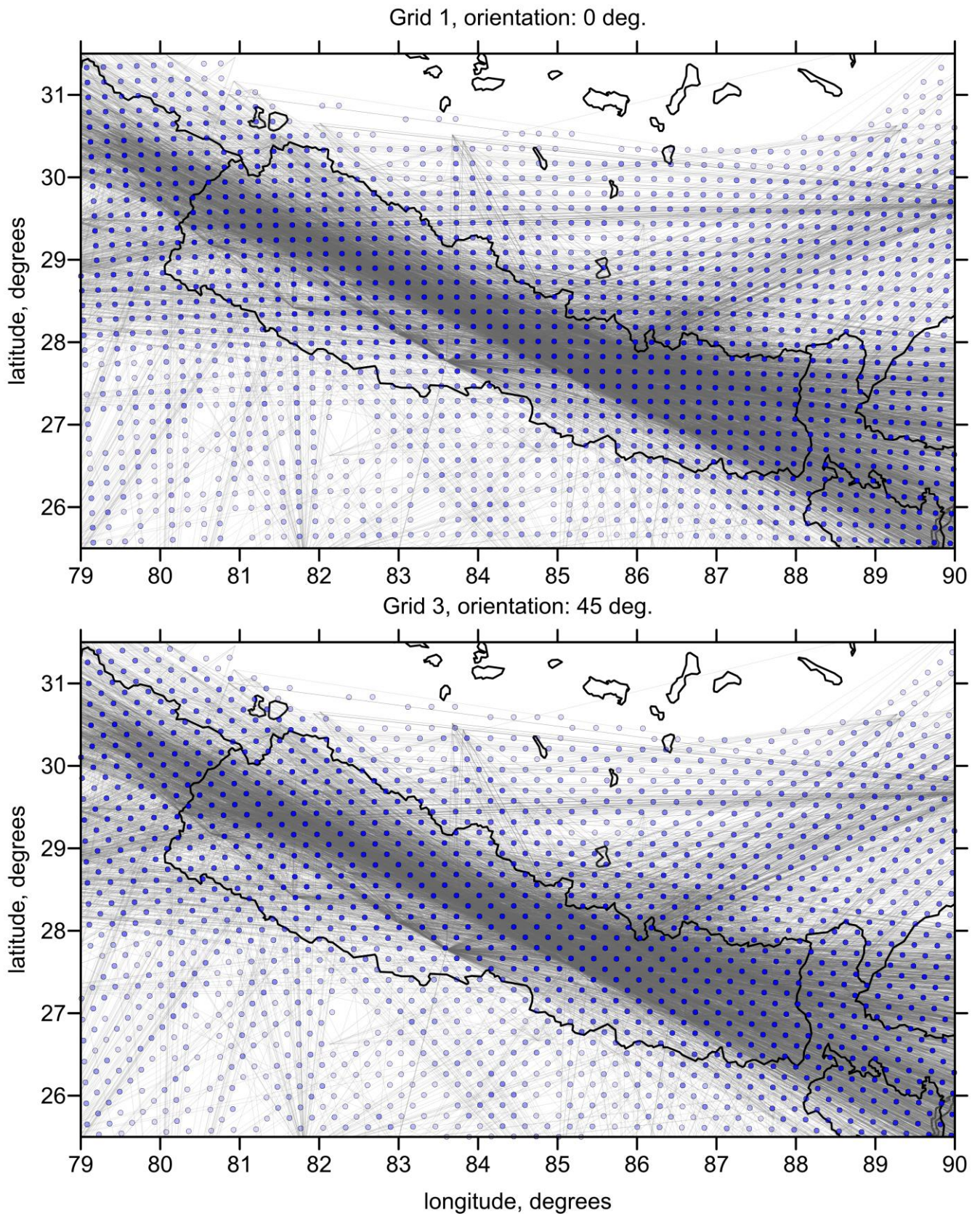
Figure 2. Distribution of P-rays and two parameterization grids corresponding to basic orientations of 0 and 45 degrees. Intensity of the points represents the number of nodes in Z-direction corresponding to the current XY coordinates.
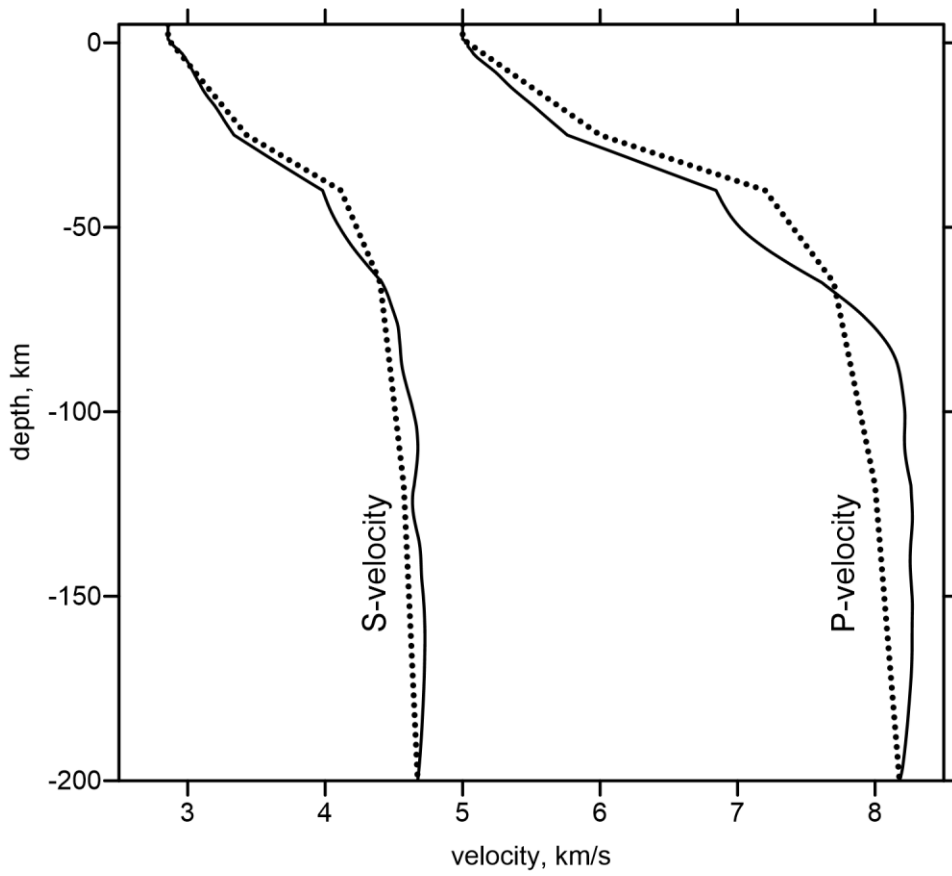
Figure 3. P- and S-velocity versus depth. Dotted lines depict starting 1D velocity models, solid line represents average velocities along section 1for the main result shown in Figures 6-7.
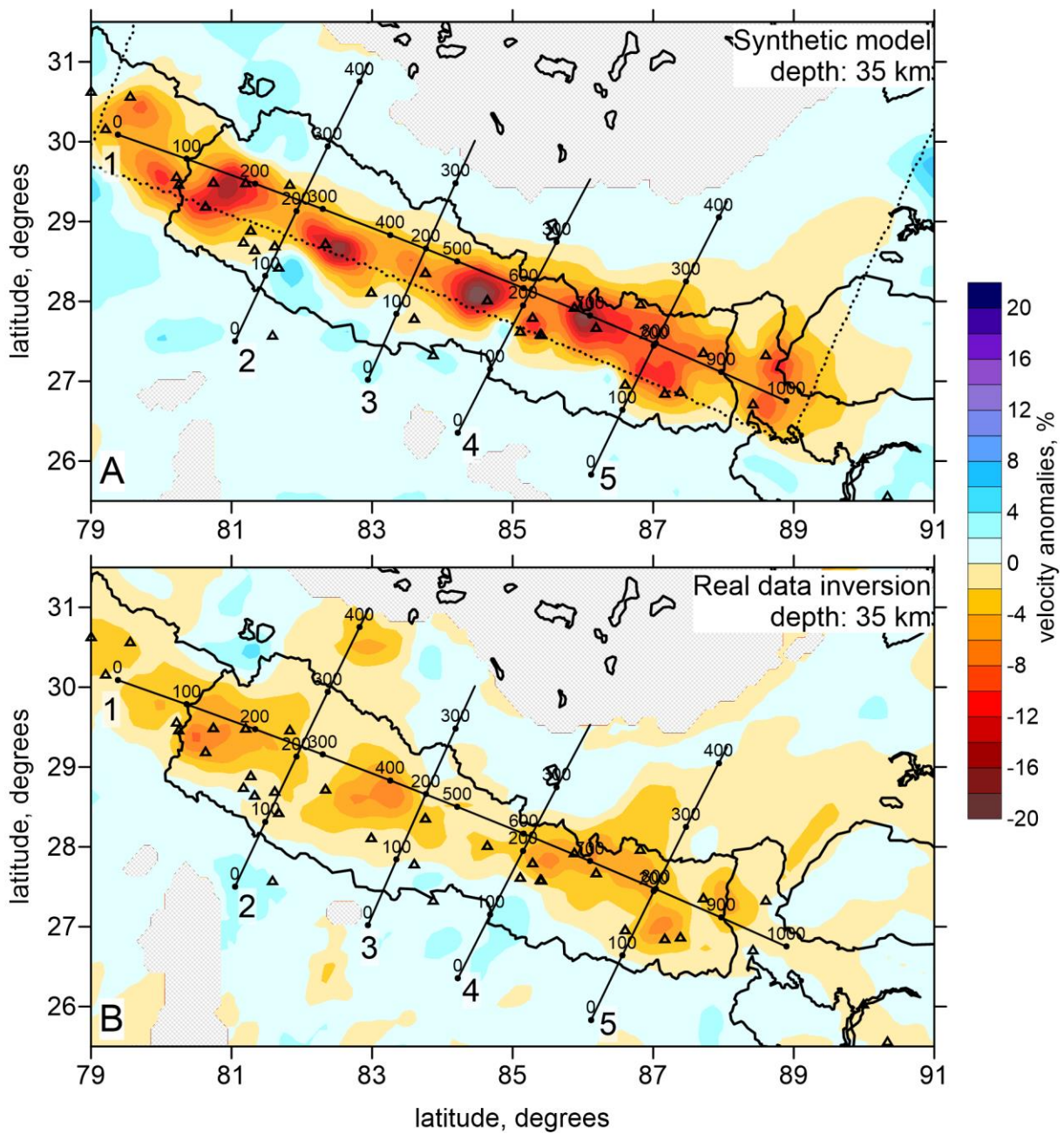
Figure 4. Velocity anomalies at 35 km depth after inversion of synthetic (A) and observed data (B). For the case of synthetic modeling, the limits of "thick crust" are marked with dotted line. Triangles denote stations. Locations of profiles presented in Figures 3 to 5 are shown.
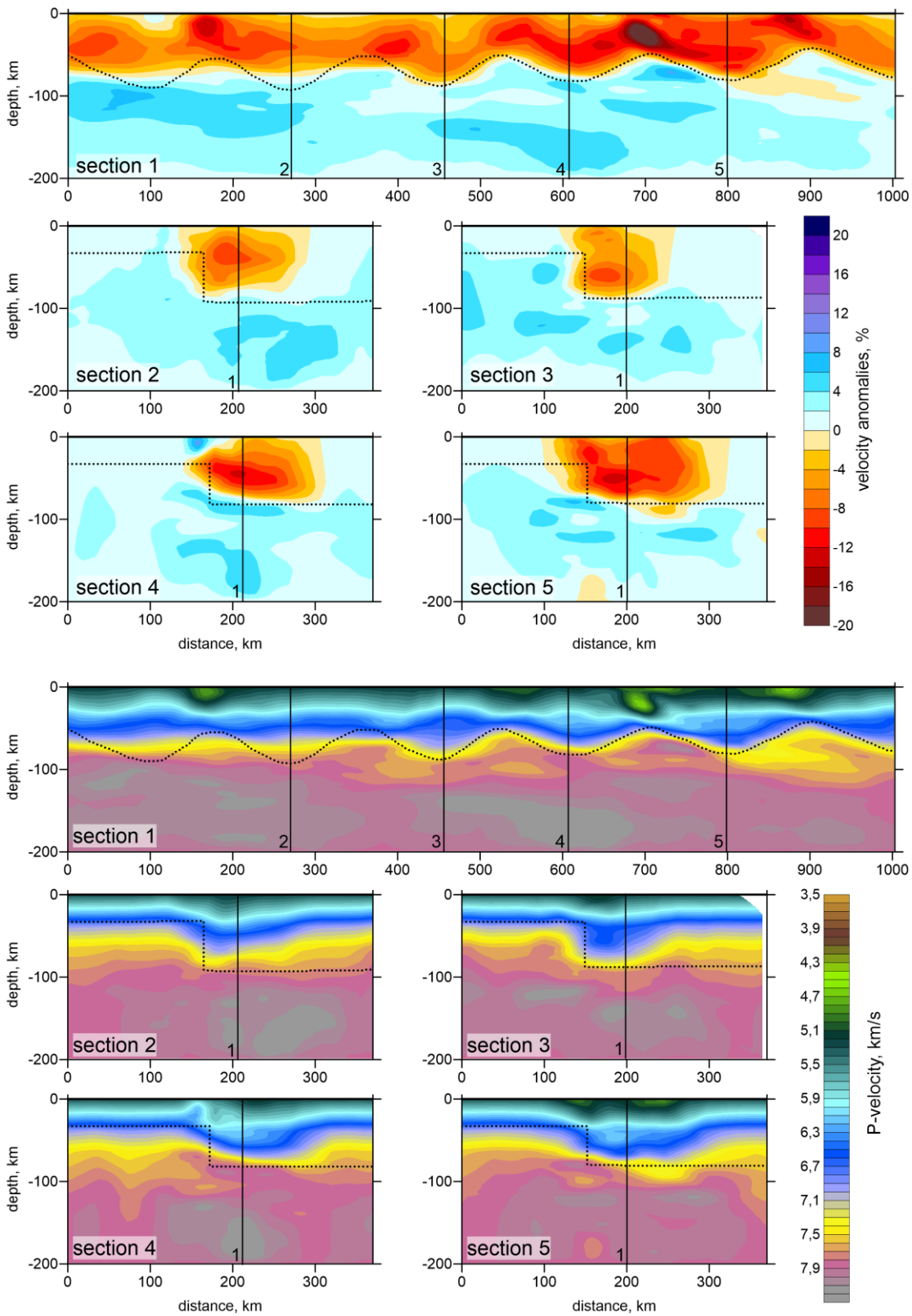
Figure 5. Synthetic test with reconstruction of the "variable Moho" model in relative anomalies (upper part) and absolute P-velocities (lower part). Locations of the profiles are shown in Figure 2. The configuration of the synthetic "Moho" is indicated with dotted line. Vertical lines with numbers mark locations where sections cross each other.
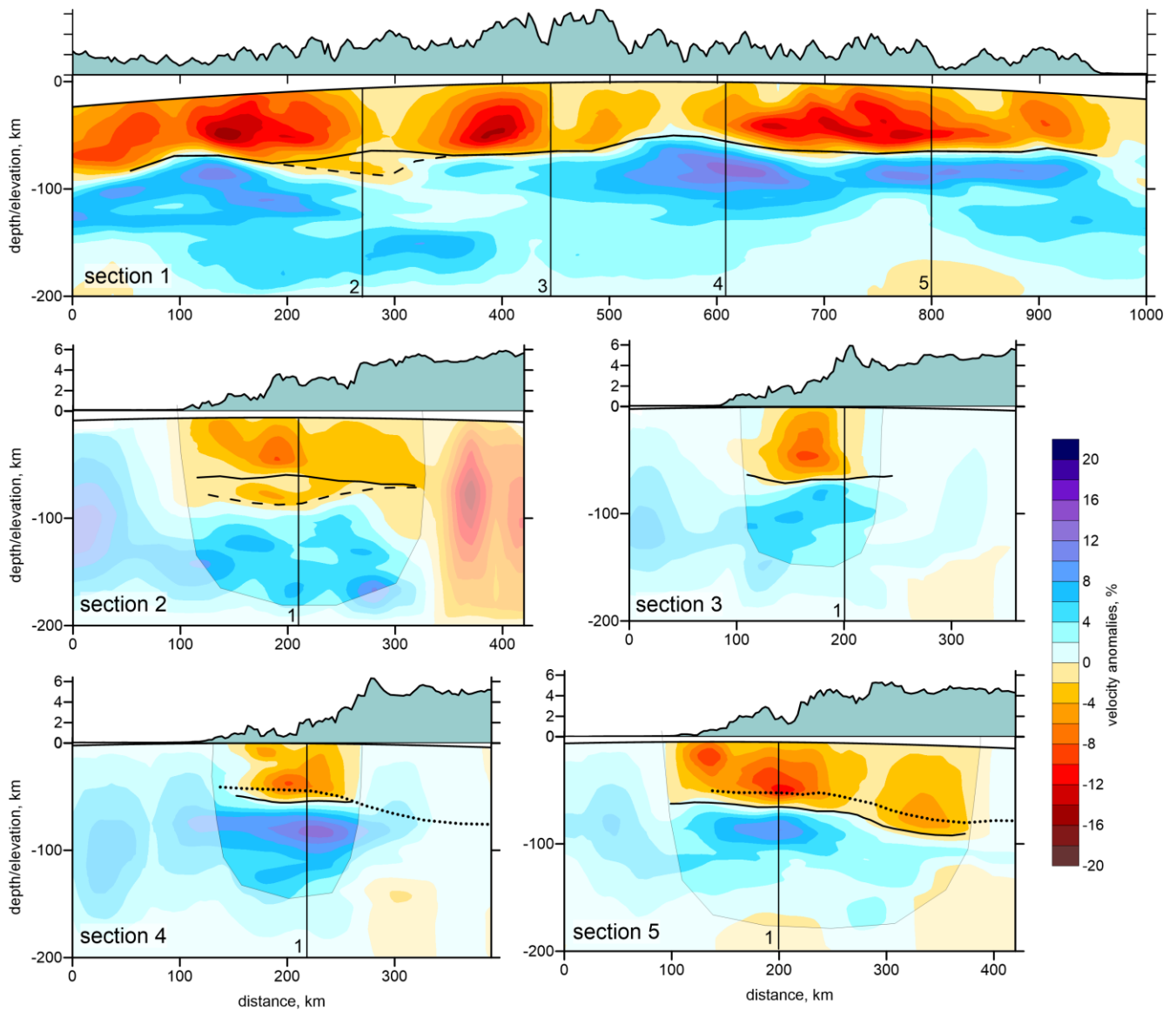
Figure 6. Vertical sections of the resulting P-velocity anomalies. Locations of sections are indicated in Figure 4. Above each section, exaggerated topography is shown. Vertical lines indicate locations where sections cross each other. Areas with poorer resolution in sections 2 to 5 are shaded. Moho interface (black line) is traced on the bottom of the low-velocity anomaly. Dashed line in Sections 1 and 2 indicates an alternative interpretation which is less plausible. Dotted lines in Sections 4 and 5 indicate Moho depth determinations from (*Hetényi et al.,* 2006) and (*Schulte-Pelkum et al.,* 2005), respectively. More sections are shown in Supplementary.
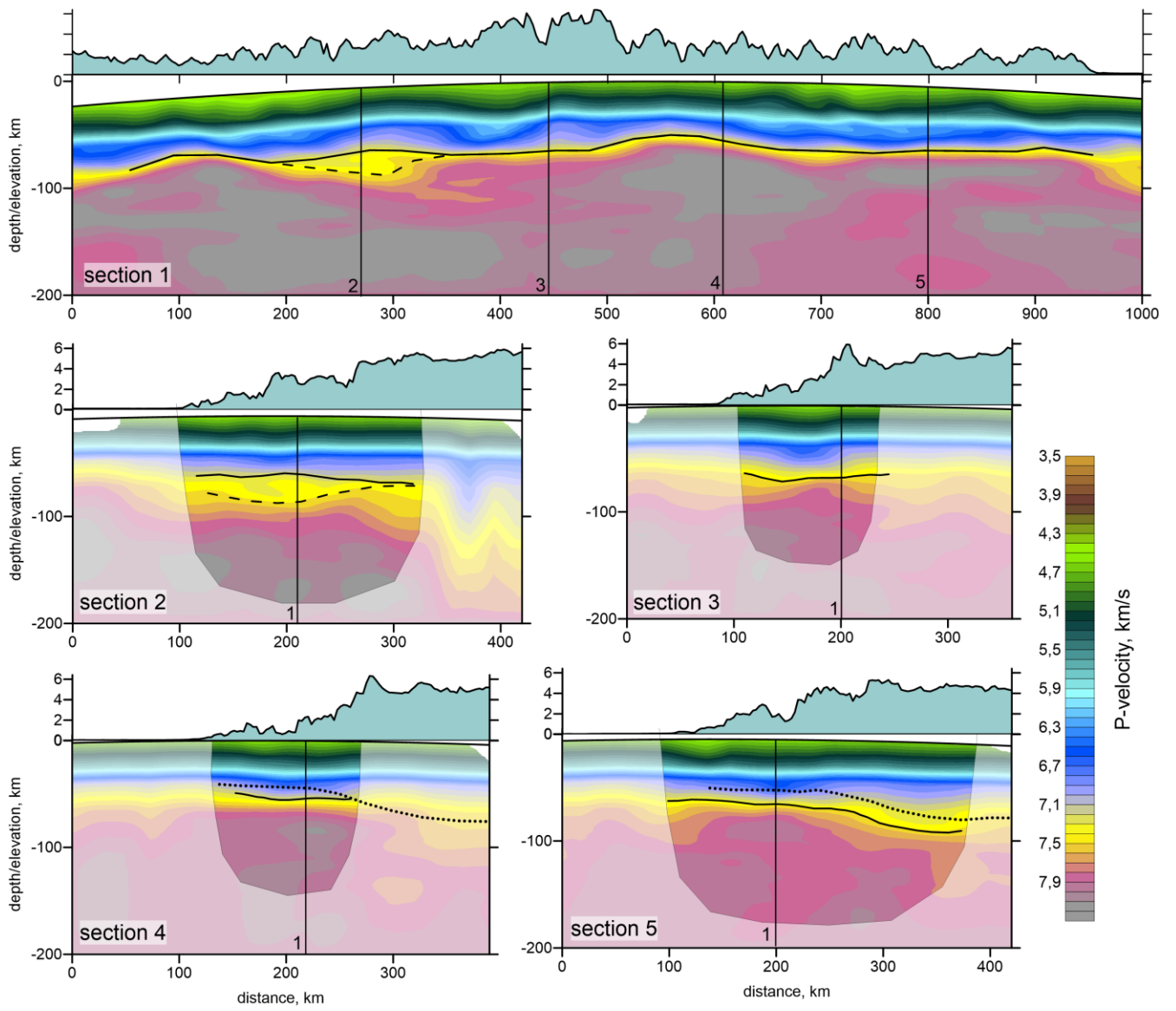
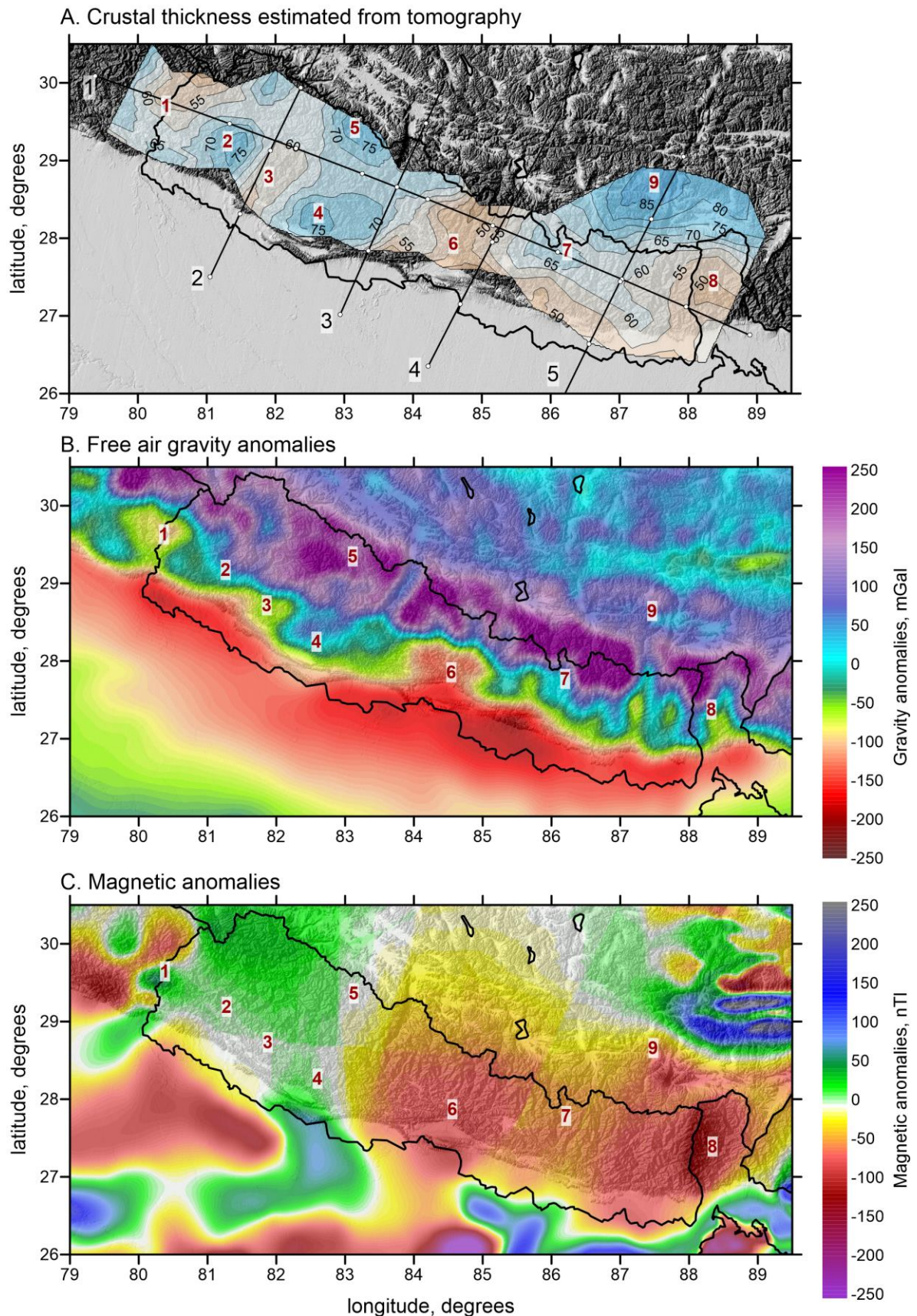Figure 7. Same as Figure 6, but for absolute P-velocity.

Figure 8. Map of estimated Moho depth beneath the Nepal Himalayas (A) together with free-air gravity anomalies (*Andersen et al., 2010*) (B) and magnetic anomalies (*Maus et al., 2009*) (C). Red numbers indicate the locations discussed in the text. In Plot A, the locations of profiles used for presenting the main results are shown.